Macromolecules

ARTICLE

pubs.acs.org/Macromolecules

Surface-Initiated Nitroxide-Mediated Polymerization from Ordered Mesoporous Silica

Hélène Blas,[†] Maud Save,[*,‡] Cédric Boissière,[§] Clément Sanchez,[§] and Bernadette Charleux[*,⊥]

[†]Laboratoire de Chimie des Polymères, UPMC and CNRS, Université Paris 6, UMR 7610, 4 Place Jussieu, 75252 PARIS Cedex 05, France

[‡]IPREM Groupe Physique et Chimie des Polymères, Université de Pau et des Pays de l'Adour and CNRS, UMR 5254, Technopole Hélioparc, 2 Av Président Angot, 64053 PAU Cedex 9, France

[§]Laboratoire de Chimie de la Matière Condensée, Collège de France, UPMC and CNRS, Université Paris 6, UMR 7574, bâtiment C−D, 11, place Marcelin-Berthelot, 75231 PARIS Cedex 05, France

[⊥]CPE Lyon, CNRS UMR 5265, Laboratoire de Chimie Catalyse Polymères et Procédés (C2P2), Université Lyon 1, Team LCPP Bat 308F, 43 Bd du 11 novembre 1918, F-69616 Villeurbanne, France

Supporting Information

ABSTRACT: This work describes, for the first time, the nitroxide-mediated polymerization (NMP) of styrene initiated from an SG1-based alkoxyamine grafted on both the inner and outer surfaces of ordered mesoporous silica (OMS) particles. The OMS particles with various morphologies were synthesized by sol−gel chemistry in the presence of a surfactant template. The initiator derived from the BlocBuilder alkoxyamine was covalently grafted via a dimethylethoxysilane functional group. The polymerizations were conducted in the presence of a free alkoxyamine with chemical structure similar to that of the grafted one. The monomer conversion was monitored by ^{1}H NMR analysis and the concentration of released nitroxide could be calculated, providing an estimation of the fraction of dead chains. The weight fraction of grafted polymer and the molar mass distributions of the free and grafted chains were determined. From this information, an effect of the OMS particle structure on the outcome of the polymerization could be evaluated.

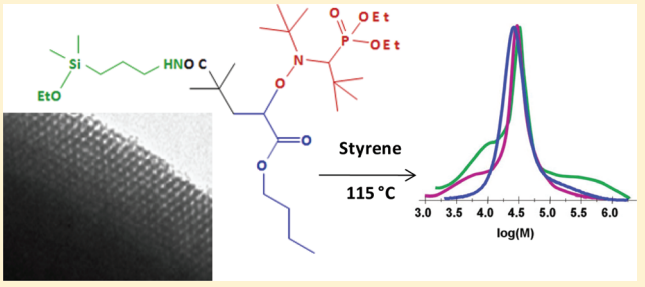

INTRODUCTION

Surface-initiated controlled radical polymerization (SI-CRP) from inorganic materials has been widely studied with the aim of producing a well-defined polymer layer at the surface, with a good control over thickness and surface density.[1,2] In comparison to colloidal particles such as silica,[3,4] or planar surfaces such as silicon wafers,[4] SI-CRP from ordered mesoporous silica (OMS) particles has been much less investigated. It was reported in the literature as a way to produce well-defined hybrid materials for various applications.[5−7] These hybrid materials usually aimed at taking advantage of the mesoporosity of the particles, combined with the properties of the polymer layer.

Surface-initiated atom transfer radical polymerization (SI-ATRP)[8−10] of monomers leading to thermosensitive polymers was performed from mesostructured silica in order to synthesize smart materials for the controlled release of fluorescein[5,6] or ibuprofen.[7] For a different purpose, SI-ATRP of acrylonitrile was performed by Kruk et al.[11] from FDU-1 and SBA-15 mesoporous silica, to fill the inner porous volume; after carbonization and elimination of the silica template, mesoporous carbon was obtained. Oligomers of methyl methacrylate (5 to 15 units) synthesized by SI-ATRP were later employed by Sherrington et al. to modify the pore surface of SBA-15 particles,[12] while preserving part of the inner porous volume. RAFT (reversible addition−fragmentation transfer)[13−15] agents were grafted on the outer surface of OMS particles, and acrylic acid[16] or *N*-isopropylacrylamide[17,18] were subsequently polymerized, affording hybrid nanoparticles with a polymer shell sensitive to pH or temperature. The RAFT agent was mainly grafted on the outer surface because the reaction was performed in the presence of the surfactant template, and no polymerization could thus take place inside the pores. Lenarda et al.[19] performed the surface-initiated nitroxide-mediated polymerization (SI-NMP) of styrene from MCM-41 mesoporous silica particles previously grafted by a styryl−TEMPO alkoxyamine. However, no macromolecular characteristics of the grafted chains were provided.

It appears from the literature data that CRP initiated from an OMS surface in such a confined environment was not straightforward and there is still a lack of information on the polymerization kinetics inside the pores and on the grafted polymer chain

Received: February 15, 2011
Revised: March 21, 2011
Published: March 30, 2011

characteristics. The currently available results are actually all based on ATRP. For instance, our team performed the detailed analysis of SI-ATRP[20] of methyl methacrylate and styrene from MSU mesoporous particles exhibiting cylindrical pores (diameter 5 nm), in the presence of a free ATRP initiator. The cleaved polymer chain features were relatively similar to those of the free chains, which was usually expected for SI-CRP initiated from dense spherical particles.[10,21−25] The polymerizations were conducted to relatively high conversions and the grafted poly(methyl methacrylate) (PMMA) and polystyrene (PS) displayed a dispersity of 1.13 (conversion 43%) and 1.23 (conversion 85%) respectively. Another study led to the synthesis of hybrid multistructured mesoporous particles[26] of various morphologies grafted by poly(methyl methacrylate). The final materials showed very high polymer contents up to 90 wt % and no residual porosity, as the polymer filled the pores. Kruk et al.[27] reported the SI-ATRP of acrylonitrile and styrene from SBA-15 and FDU-1 mesoporous silica particles. SBA-15 silica was characterized by 10 nm wide cylindrical pores in a 2 dimensions hexagonal arrangement, whereas FDU-1 silica possessed spherical cubically ordered pores with a diameter up to 14.5 nm. Polyacrylonitrile thin films grew in a controlled manner without blocking the pores and the chains cleaved from the FDU-1 silica had a low dispersity ($Đ$ = 1.06−1.34, for 28 to 61 monomer units). In contrast, even though the porous volume of SBA-15 silica was higher than that of the FDU-1 particles, the pores were blocked more quickly during the SI-ATRP of acrylonitrile under the same conditions, while the dispersity of the grafted polymer increased. The SI-ATRP of styrene from the same substrates gave even less satisfying results and higher dispersities than that of polyacrylonitrile. In a recent study, Kruk et al.[28] described the grafting of PMMA by ATRP with activator regenerated by electron transfer (ARGET ATRP) from SBA-15 silica exhibiting large mesopores (14 and 22 nm). The dispersity of the grafted chains increased up to 2.1 with the increase of the polymer molar mass. The grafting densities and initiator efficiencies were 2 to 3 times lower than those observed earlier for polyacrylonitrile grafted via normal ATRP.[27] A thorough study of the SI-ATRP[29] of methyl methacrylate and styrene from mesoporous particles providing a wide range of pore sizes (2.5−14.5 nm) and morphologies was then reported by our team. It was shown that the grafted polymer displayed a significant population of low molar mass chains corresponding to dead species, along with a population of living chains. Genzer calculated that the concave nature of a porous substrate might increase the dispersity of grafted polymer chains,[30] due to confinement of the radicals and steric hindrance.

The results described above highlight all the complexity of SI-CRP from mesoporous substrates. Along with the usual issues of SI-CRP from dense substrates,[21,31] such as the initiator and deactivator concentrations or the initiator efficiency, the porous nature of OMS brings new parameters, such as diffusion of the reactants. In addition to the high specific surface area and high porous volume of the substrate, the morphology of the pores, their connectivity and their diameter may be very important to ensure the control of the polymerization.

Because of the particular features of SI-ATRP (i.e., need for a transition metal complex catalyst: Cu(I) activator to produce the radicals from the grafted alkyl halide initiator and Cu(II) deactivator to turn the propagating macroradical into dormant chain), the diffusion processes should have a significant impact on the outcome of the polymerization.[32,33] For this reason, we were interested in studying SI-NMP,[34−39] in which the production of radicals from the surface results from a simple thermal activation of the grafted alkoxyamines. NMP is a reversible termination CRP technique, which relies on the deactivation of the growing polymer radical by a nitroxide.[34,40] The simplicity of NMP is thus considered as an advantage for the better understanding of surface-initiated polymerization mechanisms from mesoporous substrates. SI-NMP has actually proven to be a useful tool for the functionalization of dense silica particles.[24,25,41−50] Herein, a study of the SI-NMP of styrene controlled by the nitroxide SG1 from various mesoporous substrates is detailed. The mesoporous particles employed in this work correspond to those used previously in our group for SI-ATRP.[20,26,29] The influence of the morphology of the substrate on the polymerization kinetics, on the average molar mass and molar mass distribution (MMD) of the free and grafted chains is investigated.

EXPERIMENTAL PART

Materials. Styrene (St, Acros, 99%), *n*-butyl acrylate (Aldrich, 99%) and toluene were distilled from calcium hydride prior to use. All other reagents, tetraethoxysilane (TEOS, Fluka, >99%), cetyltrimethylammonium bromide (CTAB, Aldrich, 99%), Pluronic P123 (poly(ethylene oxide)-*b*-poly(propylene oxide)-*b*-poly(ethylene oxide) triblock copolymer, $M_n \approx 5800$ g·mol^{-1}, Aldrich), Brij 56 (poly(ethylene glycol) hexadecyl ether, $M_n \approx 680$ g·mol^{-1}, Aldrich), sodium fluoride (NaF, Prolabo, 98%), ethanol (VWR, 99.5%), ammonia (30% in water, Carlo Erba), dimethylformamide (DMF, Carlo Erba, 99.9%), *N*-hydroxysuccinimide (NHS, Aldrich), dicyclohexylcarbodiimide (DCC, Aldrich), 3-aminopropyldimethylethoxysilane (APDMES, 99%, ABCR), dichloromethane (VWR), tetrahydrofuran (VWR), tert-butanol (Aldrich), hydrofluoric acid (HF, 49% in water) were used as received. The alkoxyamine BlocBuilder and the nitroxide SG1 were kindly provided by Arkema.

Preparation of Ordered Mesoporous Silica (OMS) Particles. The OMS particles **MSU-Brij56** and **SBA-15** were synthesized according to already published protocols[51−53] and the experimental procedures are detailed in the Supporting Information. The core−shell spherical silica nanoparticles (**CSSN**) with dense silica core and ordered mesoporous silica shell with mesopores oriented perpendicular to the surface were synthesized via a two-step procedure.[54] First, the spherical dense core was prepared via the Stöber protocol[55] (see Supporting Information). Then, the formation of the mesoporous shell was performed as follows. For the **CSSN50** particles, a mixture of 400 mL of water and 60 mL of CTAB solution (110 mM, 40 mL of water, 20 mL of ethanol) was prepared. The crude suspension (200 mL, 1.95 wt % silica) of the Stöber spherical silica nanoparticles (S) was added to the prepared mixture and stirred for 30 min at room temperature. Then, TEOS (4.0 g) was slowly introduced and the reaction was performed at room temperature overnight. The TEOS:CTAB:NH_3:EtOH:H_2O molar ratio used in the present synthesis was 1:0.34:7.0:168:1320. The average thickness of the mesoporous shell was 50 nm. The **CSSN20** and **CSSN70** particles were synthesized according to a similar procedure, using various quantities of TEOS (see Supporting Information). The average thicknesses of the mesoporous shells were 20 and 70 nm for the **CSSN20** and **CSSN70** particles, respectively. The particles were collected by centrifugation (8000 rpm, 10 min), dried for one night at 80 °C and calcined at 500 °C for 10 h. Characteristics of the ordered mesoporous silica particles are given in Table 1.

Synthesis of the NMP Alkoxyamine Initiators. The alkoxyamine **1** (Scheme 1) was synthesized according to the procedure described previously by Nicolas et al.[56] In a round-bottom flask were introduced 1.0 g of distilled *n*-butyl acrylate (7.8 mmol, 1 equiv), 3.0 g of

Table 1. Characteristics of the Ordered Mesoporous Silica Particles Used in This Work

name	particle morphology	mesopore ordering	D_{pore},[a] nm	D_{core}, nm	S_{spe},[a] $m^2 \cdot g^{-1}$	V_p,[a] $cm^3 \cdot g^{-1}$
S	Stöber spherical silica particles.	/	/	340	8.9	/
CSSN20	core−shell spherical nanoparticles Monodisperse (shell thickness =20 nm)	radial	2.1	410	210	0.16
CSSN50	Core−shell spherical nanoparticles monodisperse (shell thickness =50 nm)	radial	2.2	400	315	0.32
CSSN70	core−shell spherical nanoparticles. monodisperse (shell thickness =70 nm)	radial	2.4	380	430	0.39
MSU	ill-defined shape (MSU-Brij56) polydisperse (500 nm to 5 μm)	2D hexagonal	5	/	760	1.07
SBA	ill-defined shape (SBA-15) polydisperse (500 nm to 5 μm)	2D hexagonal	10	/	490	0.97

[a] Data measured by nitrogen adsorption except for **S** silica. D_{pore}, mesopore average diameter; S_{spe}, specific surface area; V_p, porous volume.

Scheme 1. Synthetic Scheme for the SG1-Based Alkoxyamine Initiator 1 Used as a Free Initiator in This Work

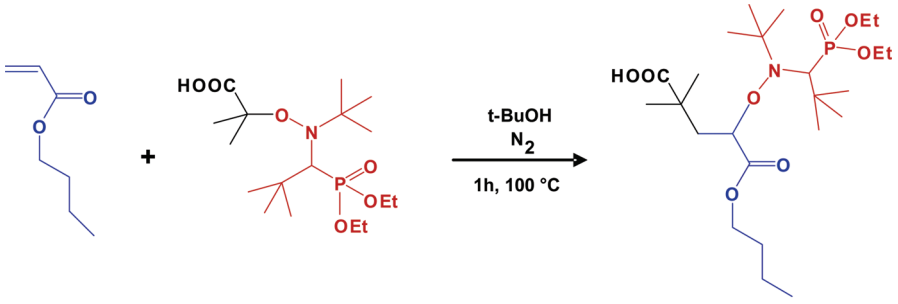

BlocBuilder alkoxyamine (7.9 mmol, 1.1 equiv), and 6.0 g of *tert*-butanol as a solvent. The reaction mixture was degassed by nitrogen bubbling for 15 min then stirred at 100 °C in an oil bath for 1.25 h. The excess *tert*-butanol was removed by evaporation, and the reaction product was precipitated in cold pentane as a white powder. Only one diastereoisomer precipitated, in a 45% total yield. NMR characterization: ^{1}H NMR ($CDCl_3$, 250 MHz, δ, ppm): 0.89 (t, 3H, $CH_3CH_2CH_2$); 1.10 (s, 9H, $(CH_3)_3CCH(P)$); 1.18 (s, 9H, $(CH_3)_3CN$); 1.22 (s, 6H, $(CH_3)_2CCOOH$); 1.29 (t, 6H, $P(OCH_2CH_3)_2$); 1.41 (m, 2H, $CH_3CH_2CH_2$); 1.69 (m, 2H, $CH_3CH_2CH_2$); 2.17 (t, 1H, $HOOCC(CH_3)_2CH_2$); 2.54 (d, 1H, $HOOCC(CH_3)_2CH_2$); 3.25 (d, 1H, J_{HP} = 26,1 Hz, *CH*P); 3.69 (m, 2H, $CH_2C(O)O$); 4.1 (m, 4H, $P(OCH_2CH_3)_2$); 4.45 (dd, 1H, $NOCH(CH_2)(COO)$). ^{31}P NMR ($CDCl_3$, δ, ppm): 24.7.

The alkoxyamine **2** was synthesized according to a procedure adapted from the synthesis of NHS-functionalized alkoxyamine by Vinas et al.[57] In a round-bottom flask were introduced 300 mg of **1** (5.9 mmol, 1 equiv), 74.6 mg of NHS (6.5 mmol, 1.1 equiv) and 10 mL of THF. The mixture was degassed by nitrogen bubbling for 5 min, then 5 mL of DCC dissolved in THF were added (146 mg, 7.1 mmol, 1.2 equiv). The solution was stirred under nitrogen at 0 °C during 2 h. At the end of the reaction, the dicyclohexylurea byproduct precipitate was eliminated by filtration. The excess THF was evaporated and **2** was precipitated in cold pentane, as a sticky solid, soluble in dichloromethane and chloroform. NMR characterization: ^{1}H NMR ($CDCl_3$, 200 MHz, δ, ppm): 0.89 (t, 3H, $CH_3CH_2CH_2$) ; 1.05 (s, 9H, $(CH_3)_3CCH(P)$); 1.13 (s, 9H, $(CH_3)_3CN$); 1.24−1.7 (6H, $P(OCH_2CH_3)_2$ − 6H, $HOOCC(CH_3)_2CH_2$ − 2H, $CH_3CH_2CH_2$ − 2H, $CH_3CH_2CH_2$); 2.23 (t, 1H, $HOOCC(CH_3)_2CH_2$); 2.66 (d, 1H, $HOOCC(CH_3)_2CH_2$); 2.74 (s, 4H, $C(O)CH_2CH_2C(O)$); 3.19 (d, 1H, J_{HP} = 31 Hz, *CH*P); 3.70 (m, 2H, $CH_2C(O)O$); 4.1 (m, 4H, $P(OCH_2CH_3)_2$); 4.56 (dd, 1H, $NOCH(CH_2)(COO)$). ^{31}P NMR ($CDCl_3$, δ, ppm): 29.9 ppm.

For the synthesis of the alkoxyamine **3**, 0.5 g of alkoxyamine **2** (8.24×10^{-1} mol, 1 equiv) and 20 g of dichloromethane were introduced in a round-bottom flask. The reaction mixture was degassed by nitrogen bubbling for 15 min. In a separated flask, 133 mg of 3-aminopropyldimethylethoxysilane (8.24×10^{-4} mol, 1 equiv) were dissolved in 5 mL of dichloromethane, under nitrogen. This mixture was added via a syringe into the first flask, and the reaction mixture was stirred for 2.5 h at room temperature. At the end of the reaction, the excess dichloromethane was evaporated under reduced pressure, and a white oil was obtained. The crude oil was dissolved in cold ether in order to precipitate the excess remaining NHS, and the alkoxyamine **3** was obtained as a transparent oil (85% yield). NMR characterization: ^{1}H NMR ($CDCl_3$, 200 MHz, δ, ppm): 0.1 (s, 6H, $(CH_3)_2Si$); 0.55 (t, 2H, $SiCH_2CH_2$); 0.89 (t, 3H, $CH_3CH_2CH_2$); 1.05−1.6 (9H, $(CH_3)_3CCHP$; 9H, $(CH_3)_3C-N$; 6H, $P(OCH_2CH_3)_2$; 6H, $HOOCC(CH_3)_2CH_2$; 2H, $CH_3CH_2CH_2$; 2H, $CH_3CH_2CH_2$; 3H, CH_3CH_2OSi; 2H, $SiCH_2CH_2$); 1.90 (m, 1H, $HOOCC(CH_3)_2CH_2$) ; 2.37 (d, 1H, $HOOCC(CH_3)_2CH_2$); 2.57 (s, 1H, *NH*); 2.87 (m, 1H, CH_2NH); 3.2 (m, 1H, CH_2NH); 3.19 (d, 1H, J_{HP} = 25.7 Hz, *CH*P); 3.53 (q, 2H, CH_3CH_2OSi); 3.81 (m, 2H, $CH_2C(O)O$); 4.10 (m, 4H, $P(OCH_2CH_3)_2$) ; 4.38 (dd, 1H, $NOCH(CH_2)(COO)$). ^{31}P NMR ($CDCl_3$, δ, ppm): 24.2 ppm.

Grafting of the Alkoxyamine 3. The mesoporous silica samples were exposed to a water saturated atmosphere during 12 h at room temperature and then dried at 100 °C under vacuum for 1 h in order to eliminate any physisorbed water in the pores. This protocol enables the creation of a maximum of silanol functions on the silica surface, thus favoring future functionalization. The silylated alkoxyamine **3** was introduced in dry toluene under a nitrogen flow (1 $mol \cdot L^{-1}$), and the

Table 2. Characteristics of the Silica Particles Functionalized with the Alkoxyamine Initiator 3

sample name	$W\%_{120-800,\ \text{initiator grafted silica}}$ [a]	$W\%_{120-800,\ \text{silica}}$ [a]	G_I [b] molecule·nm^{-2}
S-3	2.1	1.02	1.90
CSSN20−3	6.9	1.54	0.26
CSSN50−3	9.7	1.51	0.26
CSSN70−3	12.2	2.82	0.24
MSU-3	30.3	0.90	0.51
SBA-3	18.8	3.80	0.36

[a] $W\%_{120-800}$: weight loss between 120 and 800 °C (TGA analysis). [b] G_I: initiator grafting density calculated using eq 1.

solution was transferred into a purged flask containing mesoporous silica. A proportion of approximately 2 alkoxyamine molecules per nm^2 of silica surface was respected, the theoretical number of available surface silanol groups being considered equal to 5 OH/nm^2. The mixture was stirred for 12 h at 35 °C under nitrogen, then the ungrafted molecules were removed from the silica powder by five cycles of centrifugation − solvent replacement, in toluene and dichloromethane. The grafted silica was collected and dried under vacuum before characterization. See Table 2 for the characterization data.

The initiator grafting density (G_I) was calculated according to eq 1 in which W % is the weight loss between 120 and 800 °C determined by thermogravimetric analysis (TGA), N_A is Avogadro's number, $M_{initiator}$ is the molar mass of the initiator calculated by subtracting the molar mass of the −Si-OEt anchoring group, S_{spe} is the specific surface area of the mesoporous silica samples.

$$G_I = \left(\frac{W\%_{\text{initiator + silica}}}{100 - W\%_{\text{initiator + silica}}} - \frac{W\%_{\text{silica}}}{100 - W\%_{\text{silica}}} \right) \frac{}{M_{\text{initiator}} \times S_{\text{spe}}} \times N_A \ (\text{molecule/nm}^2) \quad (1)$$

Procedure for Surface-Initiated Nitroxide-Mediated Polymerization of Styrene (SI-NMP). In a typical experiment (NMP of styrene from **CSSN50** particles, **CSSN50-St** in Table 3), the initiator-grafted silica particles (401 mg, 5.4×10^{-5} mol grafted initiator, 10 mol % of the total initiator content) and free alkoxyamine initiator **1** (248 mg, 4.9×10^{-5} mol, 90 mol % of the total initiator content) were introduced in a round-bottom flask. Along with 1 g of dimethylformamide, 14.1 g of styrene were added in the flask (135 mmol, 250 equiv of the total initiator content) and the reaction mixture was degassed by nitrogen bubbling for 30 min. The polymerization was carried out at 115 °C for 300 min, and aliquots were regularly withdrawn at regular time intervals for kinetic analysis. Monomer conversion was calculated from the proton NMR spectrum of a raw aliquot using DMF as an internal standard (see Supporting Information). At the end of the polymerization, the polymer-grafted hybrid particles were recovered by centrifugation and carefully washed at least five times with dichloromethane or tetrahydrofuran. After evaporation of the excess solvents, the free polymer was analyzed by size exclusion chromatography.

The experiment **SBA-St** was carried out in three separated flasks and the polymerization was stopped at different time intervals. This procedure allowed the free and grafted chains macromolecular characteristics to be compared at each time.

The grafted polymer chains were cleaved from the hybrid silica particles using hydrofluoric acid according to the procedure described in ref 58. Dichloromethane was then added in order to dissolve the previously grafted chains, and HF was eliminated by water extraction until neutral pH. Polymer grafting density, G_P, was calculated according to eq 2, in which W % is the weight loss between 120 and 800 °C determined by TGA and $M_{n,grafted}$ is the number-average molar mass of the grafted polystyrene chains. The experimental conditions for all surface-initiated NMP of styrene are summarized in Table 3.

$$G_P = \left(\frac{W\%_{\text{initiator + silica + polymer}}}{100 - W\%_{\text{initiator + silica + polymer}}} - \frac{W\%_{\text{initiator + silica}}}{100 - W\%_{\text{initiator + silica}}} \right) \frac{}{M_{n,\text{grafted}} \times S_{\text{spe}}} \times N_A \ (\text{chains/nm}) \quad (2)$$

Characterization Methods. Proton (250 MHz) and carbon 13 (62.5 MHz) NMR analyses were performed in $CDCl_3$ using an AC250 Bruker spectrometer. The number-average molar mass (M_n), the weight-average molar mass (M_w) and the molar mass distribution (dispersity $Đ = M_w/M_n$) of the obtained polystyrene were determined by size exclusion chromatography (SEC) using tetrahydrofuran (THF) as an eluent at a flow rate of 1 mL·min^{-1}. The SEC apparatus was equipped with a Viscotek VE 5200 automatic injector, two columns thermostated at 40 °C (PSS SDV, linear M, 8 mm, 300 mm, particle size = 5 μm, mixed bed columns, separation range 10^2-10^6 g mol^{-1}, and a differential refractive index detector (LDC Analytical refractoMonitor IV). The average molar masses were derived from a calibration curve based on polystyrene standards from Polymer Standards Service (separation limits: 260 to 2×10^6 g·mol^{-1}). The hydrodynamic diameters of the particles were determined by dynamic light scattering with a Zetasizer Nano S90 apparatus from Malvern. Thermogravimetric analyses (TGA) were performed on a TGA Q50 from TA Instrument using a temperature ramp from 20 to 800 at 20 °C·min^{-1} (the weight loss is denoted W %). Fourier transform infrared (FTIR) spectra were recorded from KBr pellets at room temperature using a Nicolet Avatar FTIR spectrometer. Transmission electron microscopy (TEM) images were taken with a JEOL JEM 100CX II (100 kV) instrument. The samples dispersed in ethanol were dropped onto a carbon-coated copper grid and dried before TEM analysis. Powder X-ray diffraction (XRD) patterns were recorded by using a conventional diffractometer (Philips PW1820) operating in reflection geometry ($\theta-2\theta$ mode) with Cu (Kα) radiation (λ = 0.15418 nm). Porosity was characterized by N_2 adsorption/desorption curves obtained with a Micromeritics ASAP2010 apparatus. Surface area value and pore size distribution were obtained with the corrected BET equation and Broekhoff and de Boer models, respectively.[59] All measurements were performed on calcined powders.

RESULTS AND DISCUSSION

Synthesis and Functionalization of Ordered Mesoporous Silica Particles. The **MSU** and **SBA** ordered mesoporous silica particles were synthesized via hydrolysis/condensation of tetraethoxysilane in the presence of either poly(ethylene oxide) hexadecyl ether (Brij 56) (for **MSU**) or poly(ethylene oxide)-*b*-poly(propylene oxide)-*b*-poly(ethylene oxide) triblock copolymer (Pluronic P123) (for **SBA**) used as templates (Table 1). The **MSU** and **SBA** particles had an ill-defined shape, but an ordered arrangement of the cylindrical mesopores with a narrow pore size distribution as observed by transmission electron microscopy (Figure 1). The 2-dimensional hexagonal ordering of the mesopores was checked by powder X-ray diffraction (see Figure SI-1 in Supporting Information). The **MSU** and **SBA** particles exhibited pore diameters of 5 and 10 nm and specific surface areas of 760 and 490 m^2·g^{-1} respectively (see Table 1).

The synthesis of well-defined, submicrometric, spherical OMS particles (diameter below 550 nm) was performed to design a series of particles exhibiting an increasing ratio of the overall specific surface area over the external surface area. In this spirit,

Table 3. Experimental Conditions Used for the SI-NMP of Styrene Performed at 115 °C from Stöber and OMS Particles Grafted with the Alkoxyamine 3, in the Presence of Free Alkoxyamine 1[a]

sample name	wt % SiO_2[b]	% grafted initiator[c]	$DP_{n,th}$[d]
B-St[e]	0	0	250
S-St	10	10	256
CSSN20-St	3.7	8	250
CSSN50-St	2.4	10	249
CSSN70-St	2.0	10	250
MSU-St	2.6	50	249
SBA-St	5.3	50	253

[a] $[St]_0$ = 7.5−7.9 mol·L^{-1}; initial concentration of grafted and free alkoxyamines: $[\mathbf{1}+\mathbf{3}]_0$ = 30 mmol L^{-1}; [DMF] = 1.1−1.6 mol·L^{-1}. [b] Weight fraction of silica in the polymerization medium. [c] Molar ratio of grafted initiator **3** compared to the total alkoxyamine content = $[\mathbf{3}]_0/[\mathbf{1}+\mathbf{3}]_0$ [d] $DP_{n,th} = [St]_0/[\mathbf{1}+\mathbf{3}]_0$ is the theoretical number-average degree of polymerization at full conversion. [e] Model bulk polymerization of styrene conducted in the absence of silica; the initiator used was the alkoxyamine **1**.

Stöber silica particles (**S**) were used to synthesize core−shell spherical particles (**CSSN**)[26] composed of a dense silica core and an organized mesoporous shell (Figure SI-2 in Supporting Information) with mesopores having a radial orientation. Mesopore diameters of about 2 nm were obtained using cetyltrimethylammonium bromide as a template at basic pH, and the mesoporous shell thickness of **CSSN20**, **CSSN50**, and **CSSN70** samples were evaluated at 20, 50, and 70 nm, respectively, by transmission electron microscopy (see Figure 1 for **CSSN70** shown as an example). The pores exhibited a radial orientation as illustrated by the TEM images (Figure 1) and already discussed in our previous article.[60] It is thus reasonable to assume that the pore lengths are directly related to the mesoporous shell thickness. The values of the specific surface area and porous volume of each sample are gathered in Table 1.

An alkoxyamine initiator system based on the nitroxide SG1 was selected for our study. SG1 is a very efficient deactivating radical, which usually ensures a good control over the NMP of styrene.[61,62] Alkoxyamines dissociate under heating into a propagating radical and the nitroxide.[34] A 100% initiation efficiency can be attained leading to well-controlled polymer chains. The alkoxyamine **1**, used as a free (i.e., sacrificial) initiator, was synthesized by radical addition of BlocBuilder onto *n*-butyl acrylate (Scheme 1).[56] The reaction was performed in *tert*-butanol and a pure product was obtained after precipitation. This method, which exploits the difference of reactivity between alkoxyamine **1** and BlocBuilder, was previously used to synthesize functional alkoxyamines.[56,63] The silylated alkoxyamine **3** used for grafting was synthesized from **1** by modifying the carboxylic acid into an activated *N*-succinimidyl ester[42,57] to form the alkoxyamine **2**, followed by subsequent addition of 3-aminopropyldimethylethoxysilane (Scheme 2). A monoalkoxysilane reactive group was chosen in order to avoid the formation of multilayers during the grafting step. The initiator grafting densities reported in Table 2 were exceptionally high for the Stöber silica particles and remained very good for the mesoporous particles, i.e., in the 0.26 to 0.51 molecule.nm^{-2} range, which is high when considering the size of the SG1-based alkoxyamine molecule.[39] Both the alkoxyamines **1** and **3** have the same structure, which is important for

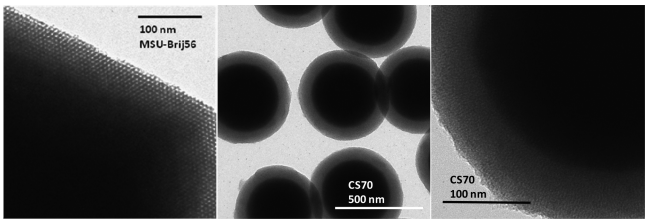

Figure 1. Transmission electron micrographs of the ordered mesoporous silica particles **MSU** (left) and **CSSN70** (middle and right) used in this work.

controlling the initiation in a similar manner in the solution (free chains) and at the surface (grafted chains). A comparable strategy based on activated ester had been proposed to synthesize silylated ATRP initiators[64] or to graft alkoxyamines.[65,66] Other methods to prepare silylated SG1-based alkoxyamines were described in the literature by Bourgeat-Lami et al.[24,45] and Billon et al.[25,67,68]

Kinetics of SI-NMP from Ordered Mesoporous Silica. The polymerization kinetics were monitored by ^{1}H NMR analysis of the remaining styrene in the samples taken at various times; for this purpose DMF was used as an internal reference (see Figure SI-3 in the Supporting Information). For the silica particles exhibiting a low specific surface area, the fraction of grafted initiator was 10 mol % (**S-St**, **CSSN20-St**, **CSSN50-St**, and **CSSN70-St**), while it was 50 mol % for **MSU-St** and **SBA-St** with large specific surface areas. In all cases, the initial overall concentration of alkoxyamine was the same, so as to target a similar chain length at full conversion (the final number-average degree of polymerization was 250). The experimental conditions are shown in Table 3 and the results are summarized in Table 4, in comparison with a model bulk polymerization of styrene conducted in the absence of silica (named **B-St**).

In all cases, for a similar polymerization time, the final conversions were not very different and the concentrations of propagating radical and released SG1 were quite comparable (in all cases the ln(1/(1-x)) versus time plots were linear, see Supporting Information). The slowest polymerization was found for **SBA-St**, while the fastest one was for **MSU-St**. The average proportion of released SG1 (also giving the proportion of dead chains)[70] was close to 20%, similar to the value found for the polymerization conducted in the absence of silica. From these kinetic results no particular trend could be found, i.e., no decisive influence of parameters such as the silica specific surface area, its overall morphology or the proportion of grafted initiator.

The free polymer chains from samples taken at various times were analyzed by size exclusion chromatography. The results are given in Table 5 and illustrated in Figure 2 for the samples **S-St**, **CSSN20-St**, **CSSN50-St**, and **CSSN70-St** and in Figure 3 for the samples **MSU-St** and **SBA-St**. For all systems except **MSU-St**, the experimental M_n points fitted well with the theoretical values and the dispersities were low, in the expected range for nitroxide-mediated polymerization.[61] These results are in agreement with a high initiator efficiency: 100% for **S-St**, **CSSN20-St**, and **CSSN70-St**, 92% for **CSSN50-St** and 87% for **SBA-St**, calculated from the ratio of $M_{n,th}$ over $M_{n,free}$. For the samples collected from the **MSU-St** experiment, the M_n data were above the theoretical line with an initiator efficiency of 71%. Also illustrated in Figures 2 and 3 are the size exclusion chromatograms of the free chains, which exhibit a very clear shift with monomer conversion

Scheme 2. Synthetic Scheme for the SG1-Based Alkoxyamine Initiator 3, Used as a Grafted Initiator in This Work

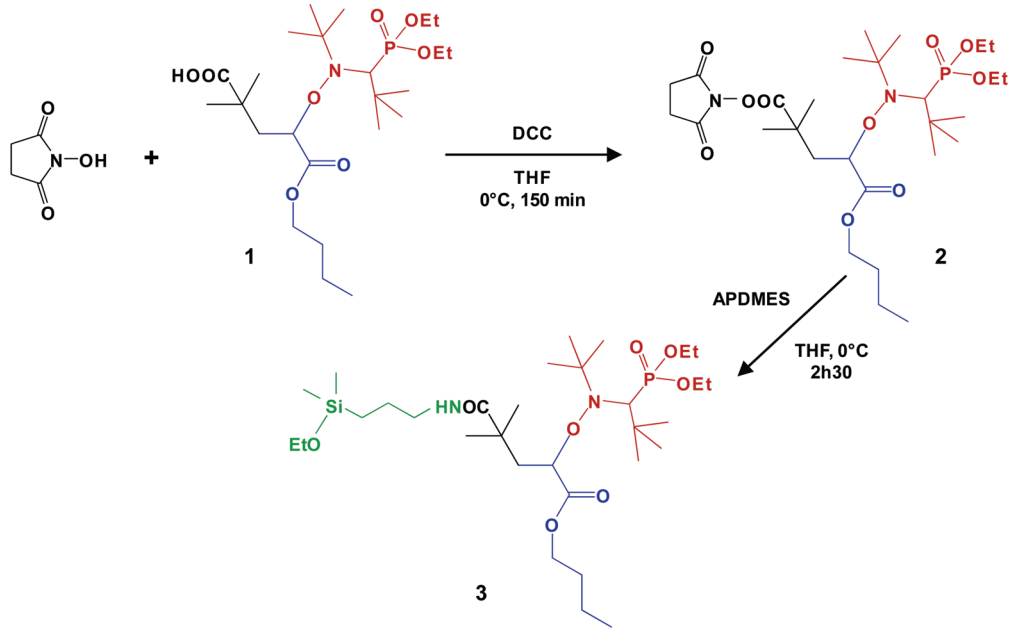

Table 4. Determination of Conversion *x*, Propagating Radical Concentration [P•], Released SG1 Concentration $[SG1]_{released}$, and Molar Ratio *R* of Released SG1 Compared to the Total Initiator Concentration for the NMP of Styrene from Various Ordered Mesoporous Silica Particles

sample name	*x* (time), % (min)	slope,[a] s^{-1}	[P•], mol L^{-1}	$[SG1]_{released}$,[b] mol L^{-1}	*R*, %
B-St[c]	65 (315)	5.6×10^{-5}	3.1×10^{-8}	6.1×10^{-3}	19
S-St	56 (300)	4.8×10^{-5}	2.7×10^{-8}	6.7×10^{-3}	22
CSSN20-St	62 (300)	5.7×10^{-5}	3.2×10^{-8}	5.8×10^{-3}	19
CSSN50-St	63 (300)	5.7×10^{-5}	3.1×10^{-8}	5.8×10^{-3}	19
CSSN70-St	62 (302)	5.9×10^{-5}	3.2×10^{-8}	5.8×10^{-3}	18
MSU-St	70 (306)	6.9×10^{-5}	3.8×10^{-8}	4.9×10^{-3}	16
SBA-St	52 (300)	4.6×10^{-5}	2.5×10^{-8}	7.0×10^{-3}	24

[a] Slope of the linear regression of $\ln(1/(1-x))$ versus time giving $k_p[P^\bullet]$ and allowing [P•] to be calculated using k_p = 1800 $L \cdot mol^{-1} \cdot s^{-1}$ at 115 °C [69]. [b] $[SG1]_{released}$: concentration of released SG1, calculated from [P•] and from the activation−deactivation equilibrium according to $[SG1] = K[\mathbf{1}+\mathbf{3}]_0/[P^\bullet]$ with *K*, the activation−deactivation equilibrium constant =6.0×10^{-9}.[61] [c] Bulk polymerization of styrene in the absence of silica.

along with a symmetrical and narrow shape, confirming the living character of the polymerizations.

In a next step, the final hybrid samples were carefully washed to remove all free chains and were analyzed by TGA to determine the amount of grafted polymer (Table 5). Upon treatment with HF to dissolve the silica component, the grafted polymers were collected and further analyzed by SEC (Table 5, Figure 4). The weight percentage of grafted initiator and polymer was low (5 wt %) for the Stöber silica with the lowest specific surface area. It increased to 35−38 wt % for the core−shell particles, was close to 60 wt % for the **SBA-St** experiment and reached a value as high as 87 wt % for the **MSU-St** experiment. From the weight percent loss values provided by the TGA analysis and assuming a density of 1 for the organic matter, one can calculate the volume (cm^3) of the organic phase per gram of pure silica (see Table 5). These values can be compared with the porous volume values V_p (calculated in $cm^3 \cdot g^{-1}$) of the particles given in Table 1. Interestingly they were always larger than V_p, indicating that the inner volume was possibly filled but that polymer chains also grew from the outer surface. The largest difference was found for the experiment **MSU-St**, in which the OMS particles exhibited the highest specific surface area and also the highest initiator grafting density.

The number-average molar mass and dispersity values of the grafted chains are reported in Table 5 and the size exclusion chromatogram overlays of the free and grafted chains are shown in Figure 4 for the experiments **S-St** and **CSSN50-St**. It appears very clearly that the grafted chains initiated from the **CSSN50** particles exhibited a broader MMD than the free ones, along with slightly higher M_n values. In contrast, for the Stöber particles, a very good overlap was observed. As shown in Figure 5, the final MMDs of the polymers grafted from all mesoporous particles were very similar: they displayed a main narrow peak shifted toward the higher molar mass values by comparison with the free chain peak, along with shoulders or tailings on both sides. The surface fraction of shoulder and tailing in comparison with the main peak depended on the type of silica substrate. The dispersity was the lowest (1.41) for the Stöber particles, it was

dx.doi.org/10.1021/ma200354r |*Macromolecules* 2011, 44, 2577–2588

Table 5. Characteristics of the Polystyrene Chains Grown from Ordered Mesoporous Silica Particles at Final Conversion (x)

sample name	x (time), % (min)	W %,[a] %	$V_{organic}$,[b] $cm^3 \cdot g^{-1}$	$M_{n,th}$,[c] g mol^{-1}	$M_{n,free}$,[c] g mol^{-1}	$Đ_{free}$	$M_{n,grafted}$,[c] g mol^{-1}	$Đ_{grafted}$	G_p,[d] chain $\cdot nm^{-2}$	G_p/G_I
B-St	65 (315)	/	/	17 400	15 850	1.14	/	/	/	/
S-St	56 (300)	5	0.05	15 400	13 650	1.18	15 000	1.41	1.4×10^{-1}	0.07
CSSN20-St	62 (302)	35	0.54	16 750	15 250	1.18	18 100	1.79	5.5×10^{-2}	0.21
CSSN50-St	63 (300)	38	0.61	16 830	17 050	1.17	16 200	2.45	5.9×10^{-2}	0.23
CSSN70-St	62 (302)	37	0.59	16 630	16 000	1.20	17 900	1.97	3.5×10^{-2}	0.15
MSU-St	70 (300)	87	6.69	18 750	24 450	1.22	24 800	2.1	2.0×10^{-1}	0.39
SBA-St	32 (120)	58	1.38	8950	11 400	1.25	13 200	5.3	7.1×10^{-2} [e]	0.20
SBA-St	47 (210)	60	1.50	12 924	13 700	1.18	15 900	5.2	9.8×10^{-2} [e]	0.27
SBA-St	53 (300)	62	1.63	14 250	15 900	1.17	15 740	7.25	1.1×10^{-1} [e]	0.31

[a] Weight loss of polystyrene-functionalized silica (i.e., initiator and polystyrene) between 120 and 800 °C, determined by TGA. [b] Volume of the organic matter per gram of silica calculated as follows: $V_{organic} = W\% / (100 - W\%)$, considering that the volumic mass of the organic part was 1 $g \cdot cm^{-3}$. [c] $M_{n,th}$, $M_{n,free}$, and $M_{n,grafted}$ are respectively the theoretical number-average molar mass, the M_n of the free chains, and the M_n of the grafted chains. [d] G_p is the polymer grafting density calculated using eq 2. [e] Poor accuracy of the PSt grafting density (G_p) due to high dispersity ($Đ_{grafted}$) of the grafted chains.

close to 2 for the core−shell (**CSSN**) and **MSU** particles, and above 5 for the **SBA-St** experiments for which the shoulders were particularly pronounced (Figure 5b).

From M_n of the grafted chains and TGA values, the polymer grafting density, G_p, was calculated via eq 2 to be below 0.2 chain $\cdot nm^{-2}$ (Table 5) for the mesoporous structures, significantly below the corresponding initiator grafting densities, G_I, reported in Table 2. Indeed, the grafted initiator efficiency calculated by G_p/G_I (Table 5) was close to 10% for the Stöber particles (with a significant error on the value due to the low amount of grafted polymer), close to 20% for the core−shell silica, close to 30% for the **SBA** particles (at final conversion) and close to 40% for the **MSU** particles.

For the **SBA-St** experiment, three runs were performed and stopped at various times to follow the free and grafted polymer chain features as a function of monomer conversion. The corresponding SEC peaks are shown in Figure 6. In this experiment, the grafted initiator efficiency varied from 0.20 at 32% conversion, to 0.27 at 47% conversion, and finally to 0.31 at 53% conversion. The MMD of the grafted chains exhibited a main narrow peak clearly shifted with monomer conversion and two large shoulders on both sides, which did not seem to change very significantly in elution volume nor in intensity with respect to the main peak. Such multimodal shape of the SEC peaks was observed in the above-mentioned experiments, but the shoulders were generally less pronounced. It was also described in ATRP systems previously studied in our group,[29] with an even larger contribution of the low molar mass shoulder compared with the main narrow peak. In that previous work, with the help of MALDI-TOF mass spectrometry analysis, the low molar mass shoulder was assigned to dead chains formed early in the polymerization process, whereas the narrow peak was attributed to living chains.[29] When the narrow peaks are compared for the grafted (Figure 6a) and the free (Figure 6b) chains, it appears that the former have their maximum (M_p) at higher molar mass. This result can be explained by different chain growth kinetics in the porous volume and in the solution, possibly due to differing concentrations of the reactants.

DISCUSSION

The polymerization kinetics were shown to be independent of the OMS particle morphology and remained close to that of the experiment performed in bulk. This is expected, considering that the initial concentration of alkoxyamine was the same in all polymerizations. However, the reactions differed in the proportion of grafted initiator (10% for the experiments **S-St**, **CSSN20-St, CSSN50-St**, and **CSSN70-St**; 50% for the experiments **MSU-St** and **SBA-St**) and in the grafted initiator efficiency (see Table 5) (the efficiency of the free initiator was considered to be 100%). In the experiments, with only 10% of grafted initiator, the grafted initiator efficiency, calculated on the basis of the G_P/G_I ratio, was approximately 20% for the **CSSN** particles, which means that 80% of the grafted alkoxyamine, i.e. 8% relative to the overall initial concentration, were not active. In consequence, the polymerization kinetics were mainly governed by the free initiator concentration. In the cases where 50% of the alkoxyamine was grafted, the grafted initiator efficiency reached 30% for the experiments **SBA-St** and 40% for the experiments **MSU-St**. Consequently, for the experiments **SBA-St**, 70% of the grafted alkoxyamine was inactive (i.e., 35% of the overall concentration), and for the experiment **MSU-St**, 60% of the grafted alkoxyamine was inactive (i.e., 30% of the overall concentration). Those last values are above the proportion R of released SG1 given in Table 4. This means that, even though all alkoxyamines should similarly dissociate under the high temperature condition of the polymerization medium, either part of the produced radicals recombine with SG1 without adding monomer units (or a very small number), or part of the released SG1 remains trapped by adsorption at the silica surface.

The highest values of the polymer grafting density, G_p, were found for the Stöber and the **MSU** particles (0.14 and 0.20 chain. nm^{-2} respectively; see Table 5). For the latter, the calculation was made considering the whole surface, which indicates a good accessibility of the inner volume to the grafting and polymerization reactions, for an average pore diameter of 5 nm, a specific surface area of 760 $m^2 \cdot g^{-1}$, a porous volume of 1.07 $cm^3 \cdot g^{-1}$ and large mesoporous particles (Table 1). In the case of the **SBA-St** experiment (pore diameter of 10 nm, S_{spe} = 490 $m^2 \cdot g^{-1}$ and V_p = 0.97 $cm^3 \cdot g^{-1}$), large mesoporous particles; Table 1), the polymer grafting density was lower and increased from 0.071 to 0.11 chain $\cdot nm^{-2}$ with the monomer conversion (Table 5). For this **SBA** silica, the initiator grafting density was also lower than that found for the **MSU** silica. Focusing now on the **CSSN** silica particles with pore diameters of 2.1 to 2.4 nm, the polymer grafting density was in the 0.04−0.06 chain $\cdot nm^{-2}$ range, whereas it was 0.24−0.26 molecule $\cdot nm^{-2}$ for the initiator grafting density, irrespective of the specific surface area and the porous volume,

dx.doi.org/10.1021/ma200354r |Macromolecules 2011, 44, 2577–2588

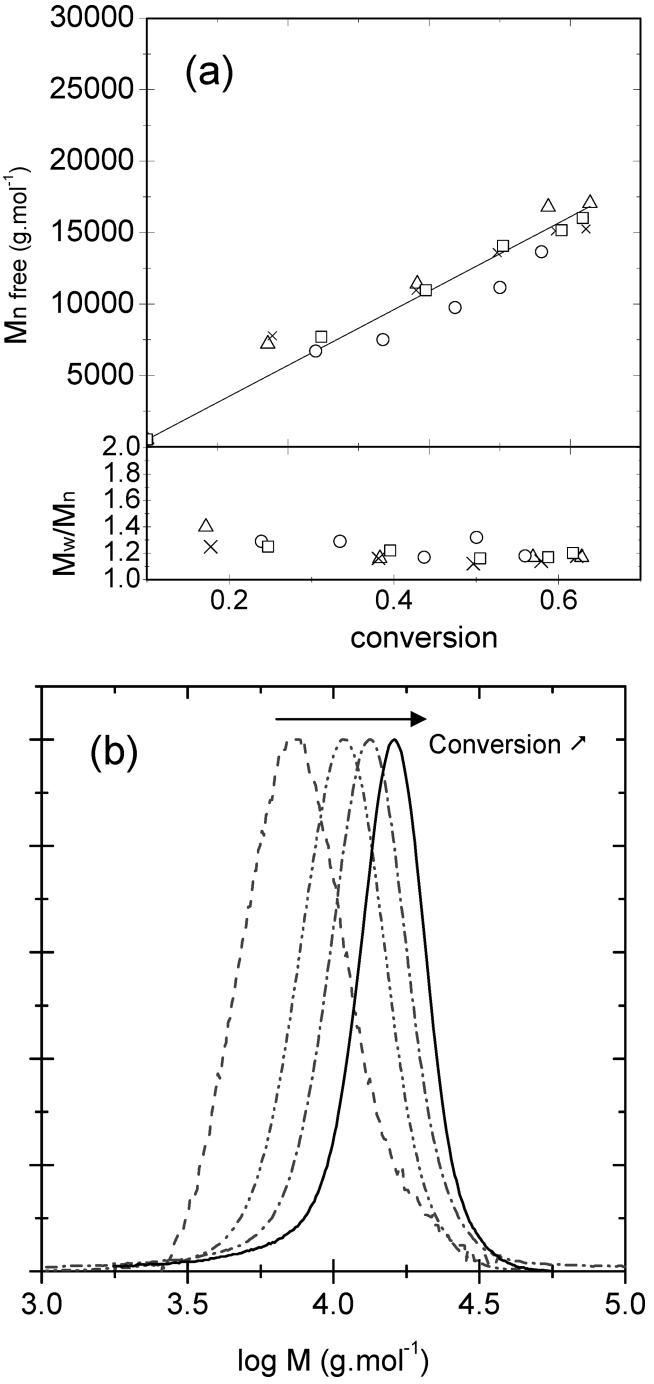

Figure 2. (a) Evolution of the number-average molar mass $M_{n,free}$ and of the dispersity $Đ = M_w/M_n$ for the free chains isolated in the polymerization of styrene in the presence of various silica particles: Stöber silica **S-St** (o), dense core−mesoporous shell silica **CSSN20-St** (×), **CSSN50-St** (Δ) and **CSSN70-St** (□), in the presence of 90 mol % of free initiator. The straight line represents the theoretical evolution of $M_{n,free}$ calculated on the basis of the overall alkoxyamine initial concentration. (b) Size exclusion chromatograms of the free chains as a function of monomer conversion for the experiment **CSSN50-St**.

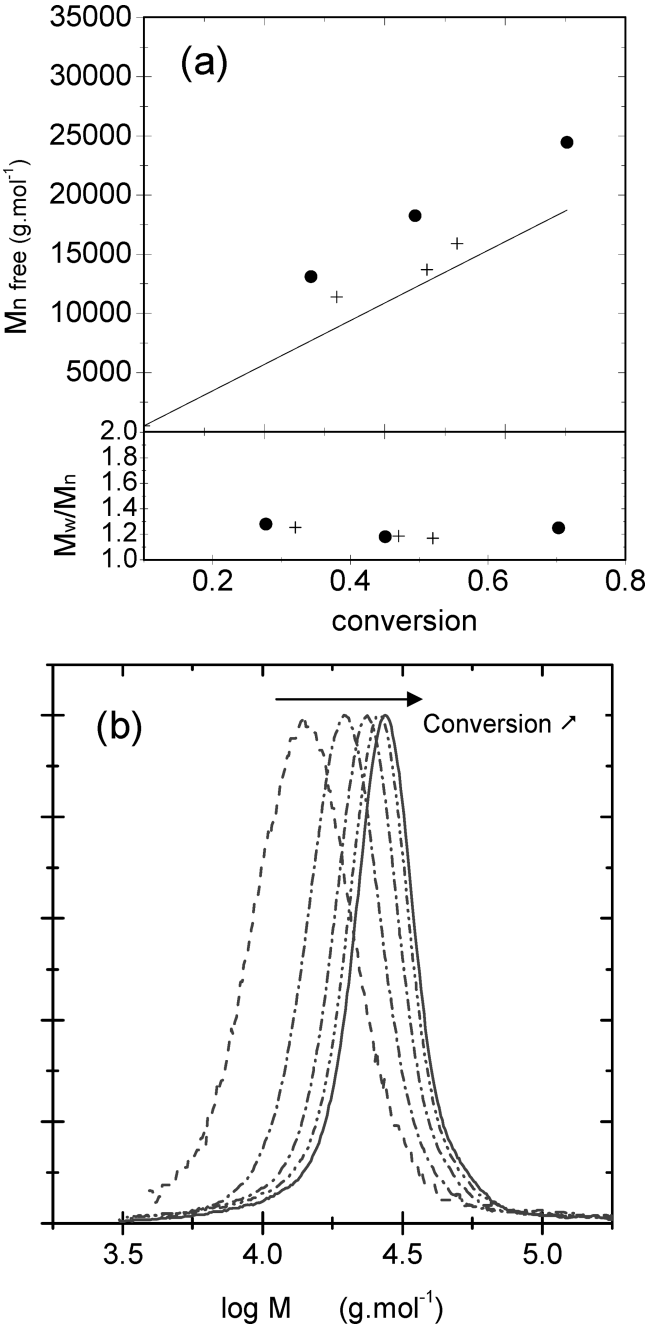

Figure 3. (a) Evolution of the number-average molar mass $M_{n,free}$ and of the dispersity $Đ = M_w/M_n$ for the free chains isolated in the polymerization of styrene in the presence of various silica particles: **SBA-St** (+) and **MSU-St** (●) in the presence of 50 mol % of free initiator. The straight line represents the theoretical evolution of $M_{n,free}$ calculated on the basis of the overall alkoxyamine initial concentration. (b) Size exclusion chromatograms of the free chains as a function of monomer conversion for the experiment **MSU-St**.

which increased with the increase from 20 to 70 nm of the mesoporous corona thickness (see Table 1). It is thus possible to conclude that the efficiency of both the grafting of the alkoxyamine and the initiation reactions do not directly depend on the average pore diameter when this one is large enough (for 5-nm diameter pores, both reactions show a better efficiency than for 10 nm-diameter pores). In contrast, for the **CSSN** particles, the polymerization results are the same irrespective of the shell thickness, indicating possible diffusion limitation that might be assigned to the small pore size. In addition, the overall particle size, i.e., the size of the porous domain, does not seem to be an important parameter for the polymer grafting density.

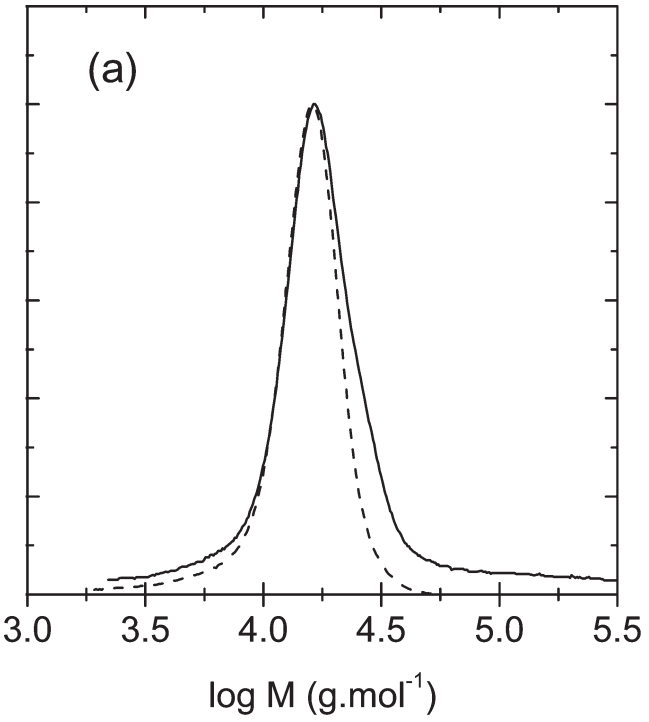

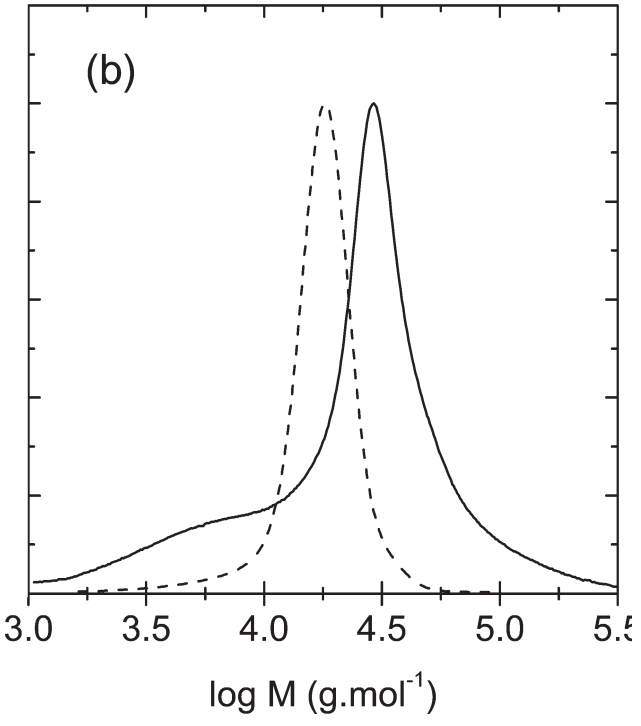

Figure 4. Size exclusion chromatograms of the final free (---) and grafted (—) polymer chains for the experiments **S-St** (a) and **CSSN50-St** (b).

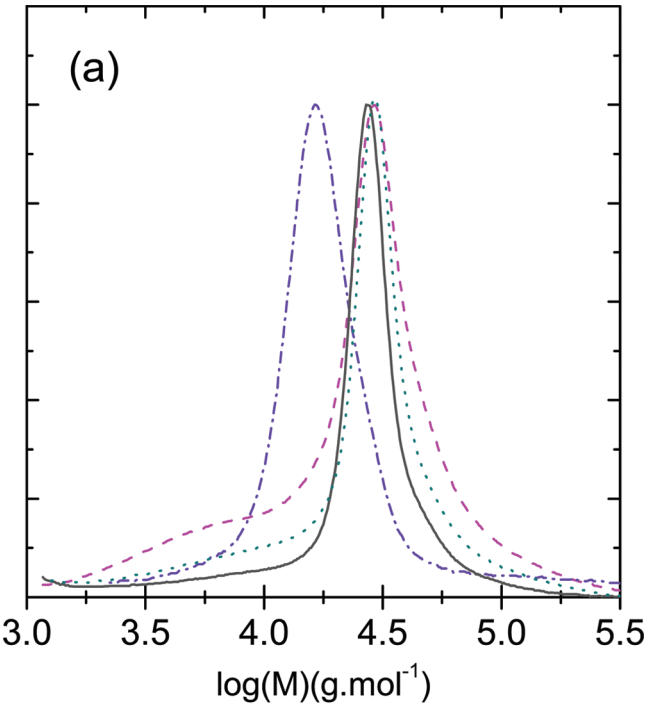

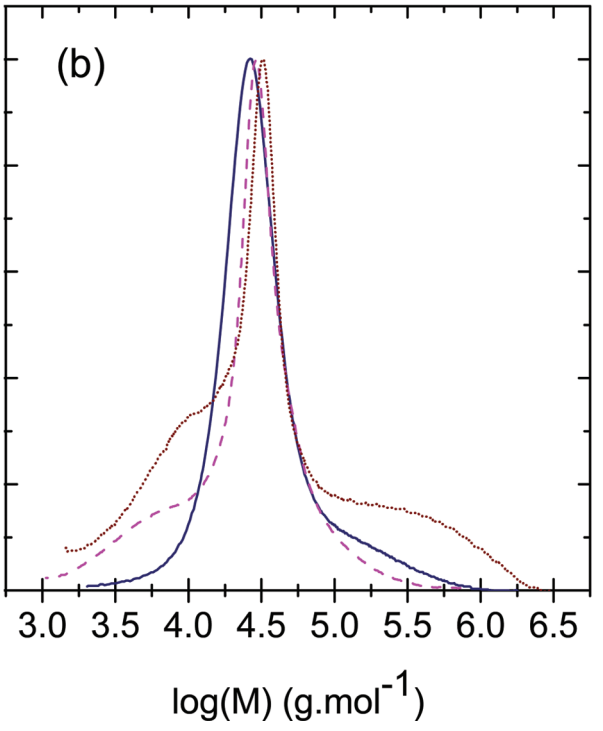

Figure 5. (a) Overlay of the SEC peaks for the final grafted chains of the experiments: **S-St** (purple —·—), **CSSN20-St** (black —), **CSSN50-St** (pink ---), and **CSSN70-St** (green ···); (b) overlay of the SEC peaks for the final grafted chains of the experiments **CSSN50-St** (pink ---), **MSU-St** (blue —), and **SBA-St** (brown ···).

The molar mass distribution of the grafted polymer had a similar shape for all OMS particles: a main narrow peak shifted toward the higher molar mass values with the progress of the polymerization, in agreement with the behavior of a living polymer, and shoulders or tailings on both sides. The proportion of the latter, in comparison with the main peak, depended on the type of silica substrate. For the Stöber particles, a narrow peak, without tailing was observed. It is thus clear that the mesoporous structure of the substrate had a significant influence on the polymer chain growth. Such a broad MMD might be related to several parameters: (i) a nonuniform concentration of SG1 in the

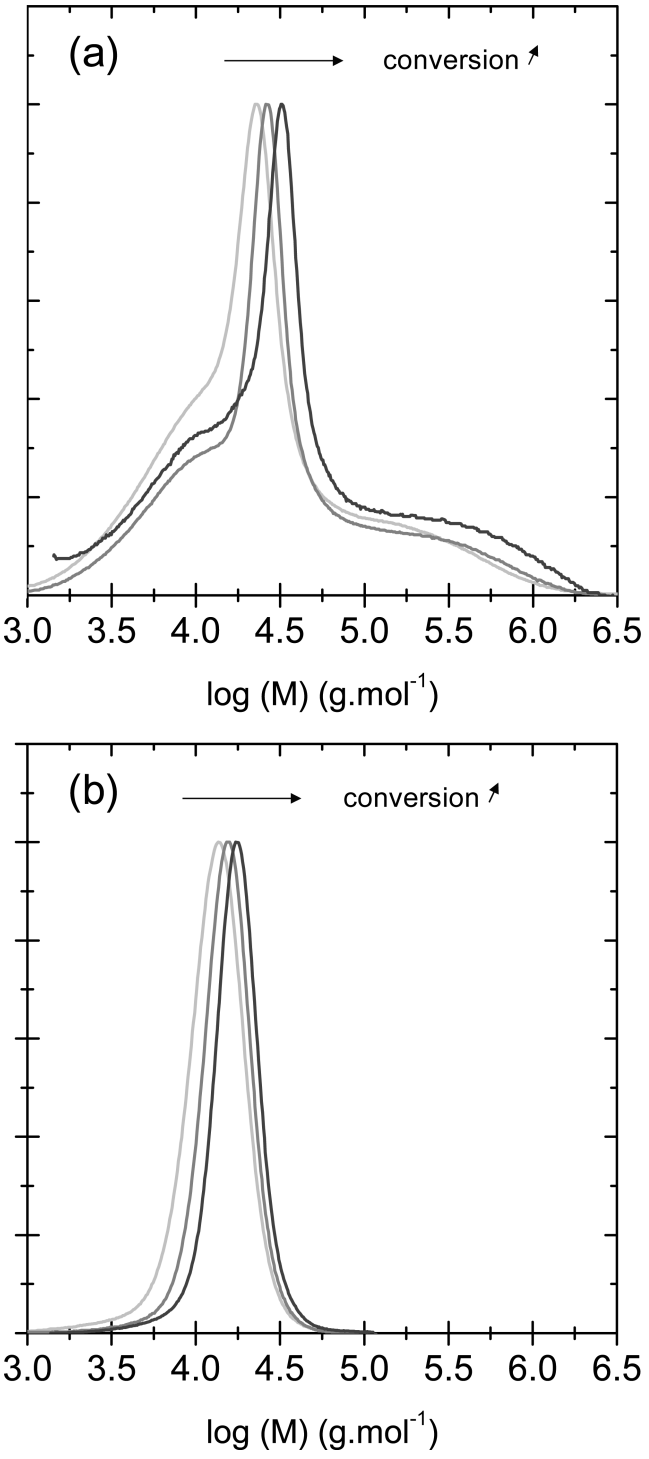

Figure 6. (a) Size exclusion chromatograms of the grafted chains for the experiment **SBA-St** stopped at various monomer conversions: 32% (light gray line), 47% (dark gray line), and 53% (black line). (b) Corresponding size exclusion chromatograms of the free chains for the same experiment.

porous volume, leading to variable lifetimes of the propagating radicals inducing the formation of short chains when the local SG1 concentration is high and long chains when the concentration is low; (ii) a nonuniform concentration of monomer affecting the local rate of propagation; (iii) a nonuniform chain mobility and/or a nonuniform radical concentration affecting the rate of irreversible termination. Surprisingly, the broadening of the MMD was the most pronounced for the **SBA** particles with significant populations of short and long chains (Figures 5 and 6), even though the pore diameter was the largest. As shown in Table 4, the experiment **SBA-St** was also the one with the highest amount of released SG1, i.e., the highest amount of dead chains. Such behavior has already been reported for SBA-15.[27] The specific porous structure of SBA-15 is probably playing a major role. In particular, the distribution of micropores strongly depends on the synthetic procedure.[71] Our **SBA** particles were specially treated in order to limit the formation of micropores (see Supporting Information) and were therefore mainly constituted of long pore channels without interconnection between them. This situation is not favorable to a rapid diffusion of the reactive species. For the **CSSN** particles with very small pore diameters, one may suspect that a major part of the polymerization takes place in a restricted volume close to the external surface of the porous shell, in which diffusion of the reactants remains possible and sufficiently fast. However, longer porous channels seem to entail a higher dispersity of the grafted chains. The pore morphology of the **CSSN** particles resembles that of **SBA** with parallel channels with few interconnections. For the **MSU** particles, the situation is the most favorable (far better than **SBA** or **CSSN**) and was also very good in previously published ATRP experiments.[20] This effect is likely to result from the combination of a large enough mesopore size and a highly connected mesoporous network.[72] Homogeneous and fast monomer and nitroxide diffusion for reaching reactive sites is thus facilitated if compared to monodimensional and noninterconnected mesoporous networks which have been proved to be less efficient for molecular diffusion.[72]

CONCLUSION

The surface-initiated nitroxide-mediated polymerization of styrene was performed from various types of ordered mesoporous silica particles with different morphologies and pore sizes, using an SG1-based alkoxyamine initiator. The polymerization kinetics were similar in all cases, even though the proportion of grafted initiator was different. The most important difference appeared in the molar mass distribution. From the results obtained in this work, it can be concluded that (i) pore diameters of 2 nm are too small to ensure a good diffusion of the reactants, while 5 nm seems to be adequate and (ii) for sufficiently large pore sizes (≥5 nm), the porous morphology of the particles is of high importance, in particular the pore connectivity. In consequence the best-suited OMS silica structure was the **MSU-Brij56** exhibiting 5 nm of mesopore diameter and a highly connected mesoporous network.

ASSOCIATED CONTENT

Supporting Information. Preparation of ordered mesoporous silica particles, X-ray diffractograms, and experimental procedures for surface-initiated nitroxide-mediated polymerization and kinetics.This material is available free of charge via the Internet at http://pubs.acs.org.

AUTHOR INFORMATION

Corresponding Author

*E-mail: (B.C.) bernadette.charleux@lcpp.cpe.fr; (M.S.) maud.save@univ-pau.fr.

■ ACKNOWLEDGMENT

French ministry of research, CNRS and ANR (Grant Number NT05-3_41901/ANR-05-BLAN-0290) are gratefully acknowledged for funding. The authors wish to express their gratitude to Arkema (Jean-Luc Couturier, Daniel Lebouvier, Stéphanie Magnet and Laurence Couvreur) for kindly providing SG1 and BlocBuilder. Both laboratories (UMR7610 and UMR7574) were involved in the European FAME network of excellence (FAME*noe*: http://www.famenoe.org/ and EMMI, the European Multifunctional Materials Institute: http://www.emmi-materials.eu/) and the Ph.D. of H.B. was performed within this framework. P. Beaunier is thanked for the TEM analyses.

■ REFERENCES

(1) Tsujii, Y.; Ohno, K.; Yamamoto, S.; Goto, A.; Fukuda, T. *Adv. Polym. Sci.* **2006**, *197*, 1–45.
(2) *Polymer Brushes*; Advincula, R. C., Brittain, W. J., Caster, K. C., Rühe, J., Eds; Wiley-VCH: Weinheim, Germany, 2004.
(3) Radhakrishnan, B.; Ranjan, R.; Brittain, W. J. *Soft Matter* **2006**, *2*, 386–396.
(4) Barbey, R.; Lavanant, L.; Paripovic, D.; Schüwer, N.; Sugnaux, C.; Tugulu, S.; Klok, H.-A. *Chem. Rev.* **2009**, *109*, 5437–5527.
(5) Fu, Q.; Rama Rao, G. V.; Ista, L. K.; Wu, Y.; Andrzejewski, B. P.; Sklar, L. A.; Ward, T. L.; Lopez, G. P. *Adv. Mater.* **2003**, *15*, 1262–1266.
(6) Yang, Y.; Yan, X.; Cui, Y.; He, Q.; Li, D.; Wang, A.; Fei, J.; Li, J. *J. Mater. Chem.* **2008**, *18*, 5731–5737.
(7) Zhou, Z.; Zhu, S.; Zhang, D. *J. Mater. Chem.* **2007**, *17*, 2428–2433.
(8) Matyjaszewski, K.; Xia, J. *Chem. Rev.* **2001**, *101*, 2921–2990.
(9) Kamigaito, M.; Ando, T.; Sawamoto, M. *Chem. Rev.* **2001**, *101*, 3689–3746.
(10) Von Werne, T.; Patten, T. E. *J. Am. Chem. Soc.* **2001**, *123* 7497–7505.
(11) Kruk, M.; Dufour, B.; Celer, E. B.; Kowalewski, T.; Jaroniec, M.; Matyjaszewski, K. *J. Phys. Chem. B.* **2005**, *109*, 9216–9225.
(12) Moreno, J.; Sherrington, D. C. *Chem. Mater.* **2008**, *20*, 4468–4474.
(13) Chiefari, J.; Chong, Y. K.; Ercole, F.; Krstina, J.; Jeffery, J.; Le, T. P. T.; Mayadunne, R. T. A.; Meijs, G.; Moad, C. L.; Moad, G.; Rizzardo, E.; Thang, S. H. *Macromolecules* **1998**, *31*, 5559–5562.
(14) Monteiro, M. *J. Polym. Sci., Part A: Polym. Chem.* **2005**, *43* 3189–3204.
(15) Moad, G.; Rizzardo, E.; Thang, S. H. *Aust. J. Chem.* **2006**, *59*, 669–692.
(16) Hong, C. Y.; Li, X.; Pan, C. Y. *J. Mater. Chem.* **2009**, *19*, 5155–5160.
(17) Hong, C. Y.; Li, X.; Pan, C. Y. *J. Phys. Chem. C* **2008**, *112*, 15320–15324.
(18) Chung, P. W.; Kumar, R.; Pruski, M.; Lin, V. S. Y. *Adv. Funct. Mater.* **2008**, *18*, 1390–1398.
(19) Lenarda, M.; Chessa, G.; Moretti, E.; Polizzi, S.; Storano, L.; Talon, A. *J. Mater. Sci.* **2006**, *41*, 6305–6312.
(20) Save, M.; Granvorka, G.; Bernard, J.; Charleux, B.; Boissière, C.; Sanchez, C.; Grosso, D. *Macromol. Rapid Commun.* **2006**, *27*, 393–398.
(21) Pyun, J.; Jia, S.; Kowalewski, T.; Patterson, G. D.; Matyjaszewski, K. *Macromolecules* **2003**, *36*, 5094–5104.
(22) Ohno, K.; Morigana, T.; Koh, K.; Tsujii, Y.; Fukuda, T. *Macromolecules* **2005**, *38*, 2137–2142.
(23) Husseman, H.; Malmström, E. E.; McNamara, M.; Mate, D.; Mecerreyes, D.; Benoit, D. G.; Hedrick, J. L.; Mansky, P.; Huang, E.; Russel, T. P.; Hawker, C. J. *Macromolecules* **1999**, *32*, 1424.
(24) Bartholomé, C.; Beyou, E.; Bourgeat-Lami, E.; Chaumont, P.; Zydowicz, N. *Macromolecules* **2003**, *36*, 7946–7952.
(25) Parvole, J.; Montfort, J. P.; Billon, L. *Macromol. Chem. Phys.* **2004**, *205*, 1369–1378.
(26) Audouin, F.; Blas, H.; Pasetto, P.; Beaunier, P.; Boissière, C.; Sanchez, C.; Save, M.; Charleux, B. *Macromol. Rapid Commun.* **2008**, *29*, 914–921.
(27) Kruk, M.; Dufour, B.; Celer, E. B.; Kowalewski, T.; Jaroniec, M.; Matyjaszewski, K. *Macromolecules* **2008**, *41*, 8584–8591.
(28) Cao, L.; Kruk, M. *Polym. Chem.* **2010**, *1*, 97–101.
(29) Pasetto, P.; Blas, H.; Audouin, F.; Boissière, C.; Sanchez, C.; Save, M.; Charleux, B. *Macromolecules* **2009**, *42*, 5983–5995.
(30) Gorman, C. B.; Petrie, R. J.; Genzer, J. *Macromolecules* **2008**, *41*, 4856–4865.
(31) Matyjaszewski, K.; Miller, P. J.; Shukla, N.; Immaraporn, B.; Gelman, A.; Luokala, B. B.; Siclovan, T. M.; Kickelbick, G.; Vallant, T.; Hoffmann, H.; Pakula, T. *Macromolecules* **1999**, *32*, 8716–8724.
(32) V. Nguyen, J.; Jones, C. W. *J. Polym. Sci., Part A: Polym; Chem.* **2004**, *42*, 1367–1383.
(33) Hong, S. C.; Matyjaszewski, K. *Macromolecules* **2002**, *35* 7592–7605.
(34) Hawker, C. J.; Bosman, A. W.; Harth, E. *Chem. Rev.* **2001**, *101*, 3661–3688.
(35) Husseman, H.; Malmström, E. E.; McNamara, M.; Mate, D.; Mecerreyes, D.; Benoit, D. G.; Hedrick, J. L.; Mansky, P.; Huang, E.; Russel, T. P.; Hawker, C. J. *Macromolecules* **1999**, *32*, 1424–1431.
(36) Devaux, C.; Chapel, J. P.; Beyou, E.; Chaumont, P. *Eur. Phys. J. E* **2002**, *7*, 345–352.
(37) Andruzzi, L.; Senaratne, W.; Hexemer, A.; Sheets, E. D.; Ilic, B.; Kramer, E. J.; Baird, B.; Ober, C. K. *Langmuir* **2005**, *21*, 2495–2504.
(38) Parvole, J.; Montfort, J.-P.; Reiter, G.; Borisov, O.; Billon, L. *Polymer* **2006**, *47*, 972–981.
(39) Ostaci, R. V.; Celle, C.; Seytre, G.; Beyou, E.; Chapel, J. P.; Drockenmuller, E. *J. Polym. Sci., Part A: Polym. Chem.* **2008**, *46* 3367–3374.
(40) Georges, M. K.; Veregin, R. P. N.; Kazmaier, P. M.; Hamer, G. K. *Macromolecules* **1993**, *26*, 2987–2988.
(41) Brinks, M. K.; Studer, A. *Macromol. Rapid Commun.* **2009**, *30*, 1043–1057.
(42) Blomberg, S.; Ostberg, S.; Harth, E.; Bosman, A. W.; Van Horn, B.; Hawker, C. J. *J. Polym. Sci., Part A: Polym. Chem.* **2002**, *40*, 1309–1320.
(43) Parvole, J.; Laruelle, G.; Guimon, C.; Francois, J.; Billon, L. *Macromol. Rapid Commun.* **2003**, *24*, 1074–1078.
(44) Bartholome, C.; Beyou, E.; Bourgeat-Lami, E.; Chaumont, P.; Lefebvre, F.; Zydowicz, N. *Macromolecules* **2005**, *38*, 1099–1106.
(45) Bartholome, C.; Beyou, E.; Bourgeat-Lami, E.; Chaumont, P.; Zydowicz, N. *Polymer* **2005**, *46*, 8502–8510.
(46) Bartholome, C.; Beyou, E.; Bourgeat-Lami, E.; Cassagnau, P.; Chaumont, P.; David, L.; Zydowicz, N. *Polymer* **2005**, *46*, 9965–9973.
(47) Li, D. J.; Sheng, X.; Zhao, B. *J. Am. Chem. Soc.* **2005**, *127* 6248–6256.
(48) Inoubli, R.; Dagreou, S.; Delville, M. H.; Lapp, A.; Peyrelasse, J.; Billon, L. *Soft Matter* **2007**, *3*, 1014–1024.
(49) Chevigny, C.; Gigmes, D.; Bertin, D.; Jestin, J.; Boué, F. *Soft Matter* **2009**, *5*, 3741–3753.
(50) Jiang, X. M.; Zhao, B.; Zhong, G. J.; Jin, N. X.; Horton, J. M.; Zhu, L.; Hafner, R. S.; Lodge, T. P. *Macromolecules* **2010**, *43*, 8209–8217.
(51) Boissière, C.; Larbot, A.; van der Lee, A.; Kooyman, P. J.; Prouzet, E. *Chem. Mater.* **2000**, *12*, 2902–2913.
(52) Zhao, D.; Feng, J.; Huo, Q.; Melosh, N.; Fredrickson, G. H.; Chmelka, B. F.; Stucky, G. D. *Science* **1998**, *279*, 548–552.
(53) Kresge, C. T.; Leonowicz, M. E.; Roth, W. J.; Vartuli, J. C.; Beck, J. S. *Nature* **1992**, *359*, 710–712.
(54) Yoon, S. B.; Kim, J.-Y.; Kim, J. H.; Park, Y. J.; Yoon, K. R.; Park, S.-K.; Yu, J.-S. *J. Mater. Chem.* **2007**, *17*, 1758–1761.
(55) Stöber, W.; Fink, A.; Bohn, E. *J. Colloid Interface Sci.* **1968**, *26*, 62–69.
(56) Nicolas, J.; Charleux, B.; Guerret, O.; Magnet, S. *Macromolecules* **2005**, *38*, 9963–9973.
(57) Vinas, J.; Chagneux, N.; Gigmes, D.; Trimaille, T.; Favier, A.; Bertin, D. *Polymer* **2008**, *49*, 3639–3647.
(58) Li, C.; Benicewicz, B. C. *Macromolecules* **2005**, *38*, 5929–5936.
(59) Prouzet, E.; Cot, F.; Nabias, G.; Larbot, A.; Kooyman, P.; Pinnavaia, T. *J. Chem. Mater.* **1999**, *11*, 1498–1503.

(60) Blas, H.; Save, M.; Pasetto, P.; Boissière, C.; Sanchez, S.; Charleux, B. *Langmuir* **2008**, *24*, 13132–13137.
(61) Benoit, D.; Grimaldi, S.; Robin, S.; Finet, J.-P.; Tordo, P.; Gnanou, Y. *J. Am. Chem. Soc.* **2000**, *122*, 5929–5939.
(62) Farcet, C.; Lansalot, M.; Charleux, B.; Pirri, R.; Vairon, J. P. *Macromolecules* **2000**, *33*, 8559–8570.
(63) Dufils, P. E.; Chagneux, N.; Gigmes, D.; Trimaille, T.; Marque, S. R. A.; Bertin, D.; Tordo, P. *Polymer* **2007**, *48*, 5219–5225.
(64) Mulhivill, M. J.; Rupert, B. J.; Hochbaum, A. *J. Am. Chem. Soc.* **2005**, *127*, 16040–16041.
(65) Chevigny, C.; Gigmes, D.; Bertin, D.; Schweins, R.; Jestin, J.; Boué, F. *Polym. Chem.* **2011**, *2*, 567–571.
(66) Parvole, J.; Ahrens, L.; Blas, H.; Vinas, J.; Boissière, C.; Sanchez, C.; Save, M.; Charleux, B. *J. Polym. Sci., Part A: Polym. Chem.* **2010**, *48*, 173–185.
(67) Parvole, J.; Laruelle, G.; Khoukh, A.; Billon, L. *Macromol. Chem. Phys.* **2005**, *206*, 372–382.
(68) Inoubli, R.; Dagréou, S.; Khoukh, A.; Roby, F.; Peyrelasse, J.; Billon, L. *Polymer* **2005**, *46*, 2486–2496.
(69) Buback, M.; Gilbert, R. G.; Hutchinson, R. A.; Klumperman, B.; Kuchta, F. D.; Manders, B. G.; O'Driscoll, K. F.; Russell, G. T.; Schweer, J. *Macromol. Chem. Phys.* **1995**, *196*, 3267–3280.
(70) Fischer, H. *Chem. Rev.* **2001**, *101*, 3581–3610.
(71) Prouzet, E.; Boissiere, C.; Kim, S. S.; Pinnavaia, T. J. *Microporous Mesoporous Mater.* **2009**, *119*, 9–17.
(72) Boissière, C.; Kümmel, M.; Persin, M.; Larbot, A.; Prouzet, E. *Adv. Funct. Mater.* **2001**, *11*, 129–135.